

# Modelling the X–ray cluster dipole and cluster contribution to the soft X–ray background

V. Kolokotronis<sup>1</sup>, M. Plionis<sup>2</sup>, P. Coles<sup>1</sup> and S. Borgani<sup>3,4</sup>

<sup>1</sup> *Astronomy Unit, School of Mathematical Sciences, Queen Mary and Westfield College, Mile End Road, London E1 4NS*

<sup>2</sup> *National Observatory of Athens, Lofos Nimfon, Thessio, 18110 Athens, Greece*

<sup>3</sup> *INFN Sezione di Perugia, c/o Dipartimento di Fisica dell’ Università, via A. Pascoli, I-06100 Perugia, Italy*

<sup>4</sup> *SISSA - International School for Advanced Studies, via Beirut 2-4, I-34013 Trieste, Italy*

4 October 2018

## ABSTRACT

We investigate the sampling and dipole convergence properties of flux–limited samples of mock X–ray clusters in relation to their underlying “parent” cluster distribution. To this purpose, we resort to numerical simulations of the cluster distribution and extract samples resembling the main observational features of X–ray selected cluster samples. The flux–limited samples, being quite sparse, underestimate the amplitude of the “parent” cluster dipole by  $\approx 15$  per cent on average for Local Group–like observers. However, the general shape of their dipole amplitude profiles are in relatively good agreement. We also calculate the expected contribution of clusters, selected according to the relevant criteria, to the soft (i.e. 0.1 – 2.4 keV) extragalactic X–ray background, using the ESO Key Project X–ray luminosity function, assuming a flat universe with vanishing cosmological constant. We obtain a value of about 10 per cent of the observed XRB flux.

**Keywords:** X–ray clusters: clustering – large scale structure of Universe – dark matter – soft X–ray Background

## 1 INTRODUCTION

Clusters of galaxies are the largest gravitationally–collapsed structures in the universe. This property makes these objects potentially useful tracers of the global matter distribution. Considerable observational effort has thus been spent in compiling cluster catalogues as free as possible from errors and selection biases. While it remains a very difficult task to construct bias–free optically–selected samples of rich clusters, selecting objects through their X–ray emission offers a cleaner possibility (e.g. Cen 1997). The powerful X–ray emission from the hot intra–cluster gas, peaked at the gravitational centre of the clusters potential wells, defines them much better than optical light and it is more directly related to their total mass, making such X–ray emitting objects prime candidates for tracers of the matter distribution on very large scales (for recent reviews see Ebeling et al. 1995; Guzzo et al. 1995; Collins et al. 1995; Gioia 1996).

The analysis we shall undertake in this paper was initially inspired by the ROSAT all–sky survey (RASS) and the follow–up work forming the ESO Key Program on southern cluster redshifts (Guzzo et al. 1995; de Grandi 1996). A number of other X–ray cluster surveys based on ROSAT are also available; the South Galac-

tic Pole project (SGP) by Romer et al. (1994) (a flux–limited sample comprising 128 X–ray clusters restricted to an area of 3100 deg<sup>2</sup>), the extensive optical follow–up work aimed at selected clusters from RASS by Allen et al. (1992) and by Crawford et al. (1995) (that accompanied and led to the X–ray compilation of the brand new Brightest Cluster Sample (BCS) by Ebeling et al. 1997b) and last but not least at all, the recent X–ray Brightest Abell–type cluster sample (XBACs), which constitute the largest all–sky flux–limited cluster sample to date (Ebeling et al. 1996b). Prior to the ROSAT mission many other X–ray projects were conducted with the aim to construct a large unbiased X–ray flux–limited cluster sample that could be used for detailed cosmological and statistical purposes (mapping the large scale structure of the universe, quantifying cluster evolution, investigating correlation function properties, establishing the X–ray luminosity function for clusters of galaxies, to name but a few).

The principal aim of this work is to investigate the disparities of dipole amplitude, structure and alignment between the X–ray flux–limited samples and their “parent” cluster distribution. We shall investigate this using ‘mock’ cluster samples generated in numerical simulations via an optimized version of the Truncated

Zel'dovich approximation (TZA; Coles, Melott & Shandarin 1993; Borgani, Coles & Moscardini 1994; Borgani et al. 1995). This study therefore complements and extends that of Kolokotronis et al. (1996) and of Tini Brunozzi et al. (1995) (TB95 hereafter) which concerned the relationship between the dipole of optically-identified clusters, that of galaxies, and that of the underlying matter distribution in simulations. The authors found that the high peaks of the density field (clusters) do trace the underlying mass dipole structure reasonably well, with a roughly constant amplitude difference corresponding to a linear biasing term, though with a relatively large observer-to-observer scatter. The degree of cluster-mass dipole correlation depends on the density threshold above which the clusters are defined and for the relatively low density threshold, which corresponds to a mean separation of  $\sim 30h^{-1}$  Mpc (similar to that of the ESO KP X-ray clusters), they found a very good correlation. However, the above cluster-mass dipole correlation starts degrading with increasing intercluster separation, or density threshold (see section 4.1 of Kolokotronis et al. 1996).

Dipole analyses have been carried out by many authors in recent years; for a complete description of the literature, see the references in Kolokotronis et al. (1996) (hereafter K96).

Using linear perturbation theory (Peebles 1980) one can relate the cluster dipole and the observer peculiar velocity to obtain an estimate of the  $\beta_c$ -parameter ( $\equiv \Omega_0^{0.6}/b_c$ , where  $b_c$  is the cluster bias parameter with respect to the mass). It is worth noting here specifically that, different classes of extragalactic objects (QSOs, AGN, galaxies, clusters of galaxies) have different relationships to the underlying matter distribution and may therefore differ substantially in their respective dipole behavior. Although this complicates the use of dipole properties as estimators of the cosmological density parameter,  $\Omega_0$ , it does allow one in principle to study the relative bias displayed by such objects (K96; Plionis 1995). Prominent among those analyses that have used X-ray selected objects as tracers of the density field are Miyaji & Boldt (1990) (X-ray AGN) and Lahav et al. (1989) (X-ray clusters).

Our subsidiary intention, having generated the mock X-ray cluster samples complete down to a certain flux limit, is to estimate their contribution to the soft X-ray Background (XRB) which, ever since its discovery (Giacconi et al. 1962), has been one of the outstanding puzzles in this field. Such an application is particularly interesting because as far as we know we will be simulating a large sample of X-ray clusters (for similar X-ray samples see also McKee et al. 1980; Piccinotti et al. 1982; Maccacaro et al. 1984; Lahav et al. 1989; Gioia et al. 1990; Edge, Stewart, Fabian & Arnaud 1990; Edge & Stewart 1991; Henry et al. 1992; Guzzo et al. 1995; de Grandi 1996; Ebeling et al. 1995; Ebeling et al. 1997b and references therein). This enables us to place tight limits on the relation between X-ray emitting clusters and the XRB in the soft energy band (0.1-2.4 keV). We also stress the fact that, a substantial number of work is dedicated to measure the contribution of X-ray objects to the hard XRB (2-10 keV). Although the availability

of data from the ROSAT satellite makes this task feasible for energies below 2 keV, the fact that both the spectrum of the XRB and the contribution of the resolved discrete component are yet to be determined, forces us to make some relatively uncertain assumptions, as we point out later.

The outline of the paper is as follows. An overview of the dipole analysis, together with techniques for an accurate determination of the inherent shot-noise errors, is presented in Section 2. We present a useful set of definitions, observational constraints and the method of reproducing reliable simulations of the relevant X-ray populations in section 3. We discuss the cluster dipole results in section 4, while an estimate of the contribution of X-ray clusters to the soft XRB in a critical density model is presented in section 5. Finally, we present our main conclusions in section 6.

## 2 DIPOLE FORMALISM

In this section we will present the method we use to calculate the peculiar gravitational acceleration induced by the distribution of matter as it is traced by clusters of galaxies.

### 2.1 Theoretical Preamble

As we discussed more extensively in K96, we need to assume the standard gravitational instability picture for all of this work. Within this picture we assume that linear perturbation theory applies and, perhaps with less justification, that a linear biasing scheme relates fluctuations in cluster numbers to fluctuations in the overall density of material, i.e.

$$\left(\frac{\delta\rho}{\rho}\right)_{\text{clusters}} = b_c \left(\frac{\delta\rho}{\rho}\right)_{\text{mass}} \quad (1)$$

(Kaiser 1984; Coles 1993). This scheme motivates the introduction of the parameter  $\beta$ , defined by

$$\beta \equiv \frac{f(\Omega_0)}{b} \simeq \frac{\Omega_0^{0.6}}{b}, \quad (2)$$

where  $f$  is the mass fluctuation growth rate in linear perturbation theory (e.g. Peebles 1980). Using linear theory we can relate velocities and accelerations. A classical case is to relate the only very accurately known observed peculiar velocity in cosmology, that of the Local group (LG) relative to the cosmic microwave background (CMB),  $\mathbf{u}(\mathbf{r})$ , to the peculiar gravitational acceleration induced upon it by the surrounding density fluctuations,  $\mathbf{g}(\mathbf{r})$ , which then, provided that the two vectors are aligned, allows  $\beta$  to be estimated via:

$$\mathbf{u}(\mathbf{r}) = \frac{2}{3} \frac{f(\Omega_0)\mathbf{g}(\mathbf{r})}{H_0\Omega_0} = \frac{\beta}{4\pi} \int \delta(\mathbf{r}') \frac{\mathbf{r}}{|\mathbf{r}'|^3} d\mathbf{r}', \quad (3)$$

where  $\delta(\mathbf{r})$  is the density fluctuations of the underlying mass distribution at position  $\mathbf{r}$ . Knowledge of  $b$  allows an estimate of  $\beta$ , if  $\Omega_0$  is given as an input parameter and vice versa. Although the assumption (1) is relatively well-motivated in a statistical sense, it may well turn out to be a poor approximation when applied on

a point-to-point basis, as required by this analysis. In fact, K96 found by comparing mass and cluster dipoles in simulations, in which  $\Omega_0$  was an input parameter, that they recovered the correct mean bias value but albeit with a large scatter (see also section 4.4).

Note that we will be using distance units in  $\text{km s}^{-1}$  and thus the  $H_0$  dependence drops. Wherever necessary, we will use  $H_0 = 100h \text{ km s}^{-1} \text{ Mpc}^{-1}$ .

## 2.2 Analysis Tools

We employ the method of moments to quantify the distribution of clusters around the observer. Having an available set of cluster positions,  $\mathbf{r}_i$ , around an observer placed at the origin, we can calculate the dipole and monopole moments as follows:

$$M = \sum_{i=1}^{N(R)} w_i \quad (4)$$

and

$$\mathbf{D} = \sum_{i=1}^{N(R)} w_i \hat{\mathbf{r}}_i. \quad (5)$$

The sum is taken over all  $N(R)$  clusters within a radius  $R$  and  $w_i$  ( $\propto r_i^{-2}$ ) are the appropriate weights, which should also take into account any sample selection effects. The monopole should increase linearly with distance  $R$  while the dipole  $\mathbf{D}$  keeps increasing until the most distant density inhomogeneity, that affects the dynamics of the observer, is taken into account. The scale at which this happens, which we denote as the convergence depth ( $R_{\text{conv}}$ ), should be within the effective depth of the catalogue if the estimated value of  $\beta$ , via equation (3) is to be reliable.

Since the samples we are interested in are flux-limited, the number of objects decreases with radial distance due to the rapidly decreasing selection function  $\phi(r)$ , defined as the number density of objects that can be seen above the limiting luminosity at distance  $r$ :

$$\phi(r) = \int_{L_{\min}(r)}^{L_{\max}} \Phi(L) dL, \quad (6)$$

where  $\Phi(L)$  is the luminosity function of the objects under study and  $L_{\min}(r) = 4\pi r^2 S_{\text{lim}}$ , with  $S_{\text{lim}}$  being the flux limit of the sample under study. In such a case the simple gravitational weights should be replaced by  $w_i \propto \phi^{-1}(r_i) r_i^{-2}$ , where the inverse selection function corrects (statistically) for the unseen portion of the luminosity function (for more details see K96 and references therein).

A word of caution is due here. Since we sample clusters up to 0.16 in redshift, we should have taken into account possible evolutionary effects of the X-ray luminosity function. Instead, we considered that the X-ray luminosity function (XLF hereafter) holds equally well for local and for distant objects which is clearly a simplification. Although this is still an open issue, there is recent evidence (Ebeling et al. 1996a; Nichol et al. 1997; Collins et al. 1997; Ebeling et al. 1997a; Romer et al. 1997 and references therein) that the cluster XLF does

not evolve at least up to  $z \sim 0.2-0.3$ . Therefore we feel that using an non-evolving XLF is a safe approximation at least for the distance range under study. Had we used an evolving XLF, this would obviously have had a direct impact on the accuracy of estimates of the contribution of X-ray clusters to the soft XRB (depending on the degree and the nature of the evolution).

The combination of the observed and predicted peculiar velocity yields an estimate of the  $\beta$ -parameter via equation (3) which is equivalent to:

$$\mathbf{u}(r) = \frac{\beta}{4\pi\bar{n}} \mathbf{D} = \beta \mathbf{V}_c, \quad (7)$$

where  $\mathbf{D}$  is estimated via equation (5) and the subscript  $c$  corresponds to cluster velocity. The importance of using an accurate estimator for the mean density of clusters is evident; there are alternative ways of constructing such an estimator and we refer the reader to K96 for details (Section 2.1). We verified that using different density estimators, the outcome is within 10 per cent of each other (see also Davis & Huchra 1982). In what follows we just estimate densities using equation (6). Note that this method only generates a reliable estimate of  $\beta$  if (i) the two vectors  $\mathbf{u}$  and  $\mathbf{D}$  are well-aligned (say within  $25^\circ$ ) and (ii) that the effective depth of the sample,  $R_{\text{max}}$ , exceeds  $R_{\text{conv}}$ . However, we should bear in mind that the very local contributions to the dynamics of the observer may not be represented in the cluster distribution, since these can be due to nearby galaxies, groups of galaxies or even voids in the local matter distribution. Such local effects can also be viewed as the cause of the observer-to-observer scatter in the linear biasing relation between the cluster and mass distributions (TB95; K96)

## 2.3 Shot Noise Effects

The sparseness with which the flux-limited cluster samples trace their underlying parent population introduce shot-noise (discreteness effects) in their dipole estimates which increase as a function of distance. The method of angular position reshuffling, used in K96 to estimate a similar effect for the *IRAS* galaxies, is not suitable in this case. Had we used the positional reshuffling method, we would have been measuring the convolution of the shot-noise introduced from the dilute sampling of the parent cluster population by its flux-limited subsample and of a sort of intrinsic parent cluster population shot-noise dipole (under the false assumption that clusters are Poisson samplers of the underlying *mass* field). In reality, since we will be inter-comparing cluster dipoles we are interested only in the former type of shot-noise which we estimate according to the formalism developed in Strauss et al. (1992):

$$|\mathbf{D}|_{\text{sn}}^2 \approx \sum_i \frac{1}{\phi_i r_i^4} \left[ \frac{1}{\phi_i} - 1 \right], \quad (8)$$

where the sum is over all clusters in the flux-limited sample. Evidently, the shot-noise dipole increases with depth and thus the amplitude of the flux-limited cluster dipole will also have a similar behavior, even beyond the true underlying dipole convergence depth. Therefore, in

order to identify this convergence depth, a parameter which is very important for a reliable determination of  $\beta$  via equation (7), we must correct the raw flux-limited dipole for the effects of shot-noise. Although the amplitude of the shot-noise dipole is easy to estimate, such a correction is not straightforward, because the shot-noise dipole direction is random and could point anywhere.

In the limit of uniform sampling we have from the central limit theorem that the three Cartesian components of the shot-noise dipole are equal and thus  $|\mathbf{D}_{\text{sn}}^{1d}| = |\mathbf{D}_{\text{sn}}^{3d}|/\sqrt{3}$ . Using a coordinate system in which the 1D shot-noise dipole is parallel to the direction of the shot-noise free dipole we have that  $|\mathbf{D}_{\text{corr}}| \approx |\mathbf{D}_{\text{raw}} \pm \mathbf{D}_{\text{sn}}^{1d}|$ . We will correct for the effects of shot-noise using  $|\mathbf{D}_{\text{corr}}| \approx |\mathbf{D}_{\text{raw}} - |\mathbf{D}_{\text{sn}}^{1d}|$  to provide maximum discreteness correction and thus a rough lower limit to the estimated cluster dipole while we will also investigate the case of no shot-noise correction which should provide an upper limit to the estimated dipole. The classical shot-noise correction,  $|\mathbf{D}_{\text{cor}}| = \sqrt{|\mathbf{D}_{\text{raw}}|^2 - |\mathbf{D}_{\text{sn}}^{3d}|^2}$  always produces results intermediate between the above limits and therefore we will not consider it further.

Finally, an estimate of the misalignment induced by the shot-noise dipole on the true underline dipole direction is given by:  $\delta\theta_{\text{sn}} \approx \arctan\left(\sqrt{\frac{2}{3}} \frac{|\mathbf{D}_{\text{sn}}^{3d}|}{|\mathbf{D}_{\text{raw}}|}\right)$  (see also Juskiewicz, Vittorio & Wyse 1990 and Lahav, Kaiser & Hoffman 1990 for dipole misalignment correction).

### 3 SAMPLES AND SIMULATIONS

We now turn to the observational properties of the X-ray cluster samples available at the present time, and the methods we use to simulate them. For more details on the observational data and motivation for this work, see Guzzo (1995), Guzzo et al. (1995) and de Grandi (1996).

#### 3.1 Properties of the Observed X-ray Cluster Samples

In order that our simulations be as closely related as possible to the available X-ray cluster data, we need to use an appropriate X-ray luminosity function and a realistic flux-limit. We use the Schechter-like form for the luminosity function as provided by de Grandi (1996) with parameters given in Table 1:

$$\Phi(L) = A \exp\left(-\frac{L}{L_*}\right) L^{-\alpha}. \quad (9)$$

Here,  $L_*$  is the characteristic luminosity,  $A$  is the overall normalization of the number-density, and  $\alpha$  is the usual power-law index. This luminosity function has been found to describe adequately a pilot sample comprising 111 X-ray clusters having redshifts between 0.02 and 0.2 above the limiting flux of  $3 \times 10^{-12} \text{ erg s}^{-1} \text{ cm}^{-2}$ . The energy band for this application is 0.5-2 keV, instead of the broader 0.1-2.4 keV, which we will be using. However, we can easily convert results (fluxes or luminosities) from the hard band to the band merely by using the conversion factor of order of 1.615, as suggested by de Grandi (private communication; see also section 3 of

**Table 1.** Parameters for the de Grandi (1996) luminosity function

Parameters	Values	Units
$A$	$2.3153 \times 10^{-6}$	$(h^{-1} \text{Mpc})^{-3} (10^{44} h^{-2} \text{erg s}^{-1})^{\alpha-1}$
$\alpha$	$1.32^{+0.21}_{-0.23}$	–
$L_*$	$0.66^{+0.218}_{-0.145} \times 10^{44}$	$h^{-2} \text{erg s}^{-1}$

de Grandi 1996 for details). Note that the above parameters of the luminosity function were derived from the original parameters of de Grandi (1996), by using the parametrised form of the Hubble constant. We prefer this conversion and consequently report results, which are  $h$ -dependent (see sections 4 and 5).

It is necessary to implement a minimum distance criterion, because nearby clusters are too extended to be identified by the present analysis software (SASS) of the ROSAT survey. Furthermore, the SASS detection algorithm implementation leads to an underestimation of the fluxes for all kinds of X-ray sources. In fact, both the pilot sample of the ESO KP and the whole ESO KP survey make also use of an alternative flux estimator (for both pointlike and extended X-ray emission), namely the steepness ratio technique (for a detailed delineation, see de Grandi et al. 1997 and references therein). Such a method greatly improves the flux incompleteness initially produced by the SASS, especially when the signal-to-noise ratio for the RASS sources is small (i.e. when photon statistics is low). Nevertheless, we adopt a value of  $R_{\text{min}} \simeq 45h^{-1} \text{Mpc}$  ( $z_{\text{min}} \approx 0.015$  as in RASS) as the minimum fiducial distance at which the sample is complete. Although the maximum luminosity used for the pilot sample is  $1.01 \times 10^{45} \text{ erg s}^{-1}$ , the most luminous X-ray cluster identified within RASS yields the enormous value of  $6.2 \times 10^{45} \text{ erg s}^{-1}$  (Schindler et al. 1995). This object appears to be incompatible with the luminosity function (equations 6 and 11). In any case, this is a preliminary estimate of this function, so that our results which are based on it, should be taken as indicative rather than definitive. Since the integration of this luminosity function is highly insensitive to  $L_{\text{max}}$  for values well above  $L_*$ , we impose an upper limit of  $1-1.2 \times 10^{45} h^{-2} \text{ erg s}^{-1}$ . The lower luminosity limit can be easily found in conjunction with  $R_{\text{min}}$  and the RASS flux limit. Using the ESO Key Project flux limit, i.e.  $S_{\text{lim}} = 3 \times 10^{-12} \text{ erg s}^{-1} \text{ cm}^{-2}$ , produces samples of few clusters, spanning a large redshift range, which therefore provide unreliable dipole estimates, principally because of the very large shot-noise uncertainties. Since we are interested in producing theoretical predictions that can be compared with future, more sensitive surveys we use a deeper flux-limit, comparable to that of the RASS SGP project, set by Romer et al. (1994) and those by Collins et al. (1995) and Guzzo et al. (1995), i.e.  $S_{\text{lim}} = 1.5 \times 10^{-12} \text{ erg s}^{-1} \text{ cm}^{-2}$ , which corresponds to  $L_{\text{min}} \approx 4 \times 10^{41} h^{-2} \text{ erg s}^{-1}$ . We do, however, have to hope that a survey with this deeper flux limit would still be adequately described by the same luminosity function. Since, the pilot catalogue as given above, reflects a quite uniform picture of the whole sampling space, it is our reasonable hope that such an alteration of the flux

limit will not affect the parameters of the luminosity function (L. Guzzo, private communication).

### 3.2 The simulations

We now briefly describe the simulations we use to generate mock samples of galaxy clusters. For a more detailed description, see Borgani et al. (1995).

Our prescription is based on an optimized version of the Truncated Zel’dovich approximation (Zel’dovich 1970; Shandarin & Zel’dovich 1989; Coles, Melott & Shandarin 1993). In this approximation, known as TZA, particles move along straight lines in response to the initial gravitational potential generated by a smoothed version of the initial density field. This describes the dynamics quite accurately up to the shell-crossing point, which is suppressed by the initial smoothing. In the simulations we use here, density and velocity potentials are reconstructed on  $256^3$  grid points in a box of  $L = 960h^{-1}$  Mpc aside. It has been shown that TZA accurately locates clusters when  $\sigma_8 < 1$  (Borgani et al 1995; Moscardini et al. 1996). Indeed, this is the case for the model we will be dealing with in this paper, a cold + hot dark matter model (CHDM hereafter) with  $\Omega_o = 1$  for the total density,  $\Omega_{\text{hot}} = 0.3$  for the hot component and  $\Omega_b = 0.013h^{-2}$  for the baryonic fraction (Reeves 1994). We also use  $h = 0.5$  for the dimensionless Hubble parameter and  $\sigma = 0.78$  for the rms fluctuation amplitude within a top-hat sphere of radius of  $8h^{-1}$  Mpc. In order to reduce the amount of shell crossing we filter the short-wavelength modes of the linear power spectrum using a Gaussian filter with radius  $R_f = 3.3h^{-1}$  Mpc. The model is normalized to COBE as in Gorski et al. (1994). We use this single model that has been shown to provide a good description of the cluster correlation and large-scale properties (cf. Klypin & Rhee 1994; Borgani et al. 1997).

In TB95 it was shown that using large simulation volumes the variance in the dipole estimates is dominated by the observer-to-observer scatter within the same realization and not by the different realizations of the same dark matter model. Therefore, in what follows, we will be using only a single realization of the model.

### 3.3 Cluster Sample Extraction

The simulation described above allow us to identify clusters with peaks of the dark matter density field and a subset of these peaks are used to generate a simulated cluster sample. In our previous analysis of cluster samples (K96), we assumed that there was a correlation between the height of the density peak and the optically defined richness of a cluster. In this work, we assume a similar correlation between the height of the peak and the cluster X-ray luminosity. To simulate realistic flux-limited samples of X-ray clusters we need the number density of their parent population which can be converted into a threshold for peak selection. This is used to generate the “parent” volume-limited catalogue of clusters. Then by imposing a flux limit, and the shape

of the ROSAT selection function we extract realistic X-ray cluster samples.

#### 3.3.1 “Parent” Cluster Catalogue (C)

By integrating the luminosity function from the proper lower to the upper luminosity limit, we can get an estimate of the mean number density of the “parent” distribution of X-ray clusters:

$$\bar{n}_c = \int_{L_{\text{min}}}^{L_{\text{max}}} \Phi(L) dL. \quad (10)$$

Taking the lower and the upper bound given in section 3.1, we obtain  $\bar{n}_c \approx 3.3 \times 10^{-5} h^3 \text{Mpc}^{-3}$ . Thus the number of “parent” clusters included within the cubic box is  $N_c \approx 28900$  and the number within an inscribed sphere of radius  $480h^{-1}$  Mpc is  $\approx 15100$  which corresponds to a mean intercluster separation of  $\bar{d}_c \approx 31.3h^{-1}$  Mpc, which is characteristic of the APM type of clusters (Dalton et al. 1994).

#### 3.3.2 The mock ‘ROSAT’ sample ( $\equiv R$ )

To simulate a ROSAT-like flux-limited X-ray cluster sample we use the selection function, defined in equation (6), from which we can predict the corresponding number of X-ray clusters above the flux limit,  $S_{\text{lim}} = 1.5 \times 10^{-12} \text{erg s}^{-1} \text{cm}^{-2}$ , lying within a shell between  $r$  and  $r + \Delta r$ , via:  $N(r) = 4\pi r^2 \bar{n}_c \phi(r) \Delta r$ . Fig. 1 shows the resulting  $\phi(r)$  as a function of distance. Notice the very long tail extending out to large distances. The maximum of  $N(r)$  turns out to be around  $z \approx 0.11$ , consistent with that predicted by the RASS (L. Guzzo, private communication). These considerations lead to a value of  $N_c \approx 1300$  clusters within our limiting redshift of  $z \approx 0.16$ . We are therefore in perfect agreement with the original survey target list of about 700-800 southern clusters (within  $z \approx 0.2$ ).

Finally we perform a consistency check, that of recovering from our simulated flux-limited samples the observed  $N - S$  distribution (de Grandi 1996) which is well-described by a power law of the form

$$N(> S_i) \approx A S_i^{-\alpha}, \quad (11)$$

with  $\alpha = 1.21 \pm 0.15$  and normalization constant  $A = 11.34_{-2.14}^{+1.80} \text{sr}^{-1} (10^{-11} \text{erg s}^{-1} \text{cm}^{-2})^\alpha$ . Using 500 random observers, a flux-limit comparable to that of de Grandi (i.e.  $S_{\text{lim}} = 3 \times 10^{-12} \text{erg s}^{-1} \text{cm}^{-2}$ ) and fitting equation (11), we find  $\alpha = 1.22 \pm 0.05$ ,  $A = 11.7 \pm 1$  in units as before and in excellent agreement with de Grandi (1996).

#### 3.3.3 A ‘test’ sample (T)

This test sample is constructed in order to study the effects of missing nearby clusters which are too extended to be picked up by the SASS identification procedure (inability of the standard analysis software system to define them as such, simply because it is point source detection algorithm, therefore it can not deal properly with extended X-ray emission; but see also section 3.1

for additional flux correction). We use exactly the same requirements as for the R-sample, but now we adopt  $R_{\min} = 7.5h^{-1}$  Mpc instead. The number of objects per simulation is only slightly affected, since we include the few clusters that lie between  $7.5h^{-1}$  Mpc and  $45h^{-1}$  Mpc (according to their mean separation we expect  $\approx 10$  clusters within these limits). This particular lower limit is dictated by the procedure with which we have identified the observers; all local properties are defined by using a top-hat sphere of radius  $7.5h^{-1}$  Mpc (for more details see TB95). Although such an inclusion increases insignificantly the total number of clusters, it does influence all dipole properties to a great extent, as expected from the  $1/r^2$  law of gravity and as we will quantify in our subsequent analysis.

### 3.4 Observer selection

From a starting list of 5000 random observers, identified on the grid, we will be selecting appropriate subsets with different characteristics depending on which particular issue we want to study.

Firstly we select only those observers for which their cluster dipole amplitude, on large scales ( $\sim 180h^{-1}$  Mpc), exceeds their shot-noise dipole. This results in 1500 such observers, which we call random observers. We imposed this last criterion since we are interested in studying dynamically ‘active’ regions, for which the dipole is well defined and a relative good diagnostic of the acceleration field.

As a second subset we are interested in defining LG-like observers. Imposing the usual LG requirements (similar peculiar velocity and local density contrast; cf. Borgani et al. 1995; Moscardini et al. 1996) we generate an insufficient number of observers to allow a meaningful statistical analysis to be performed. A more useful constraint for studying the large-scale characteristics of the cluster distribution (which we also used in K96) is furnished by the the structure of the observed Abell/ACO cluster dipole, which is of a two-step form with a significant contribution from large scales (cf. Scaramella et al. 1991; Plionis & Valdarnini 1991; Branchini & Plionis 1996). In other words, we will just assume that our “parent” X-ray cluster distribution has similar dipole amplitude and shape as the Abell/ACO optical clusters. Branchini & Plionis (1996) starting from the redshift space cluster distribution they recovered cluster true distances and peculiar velocities via a dynamical algorithm (cf. Yahil et al 1991; Strauss et al 1992). Their mean reconstructed real space cluster dipole has the following features.

- (i)  $V_C \approx 2400 \pm 800 \text{ km s}^{-1}$  ( $2\sigma$  range) and
- (ii) the usual two-step shape, with a final convergence at  $\sim 180h^{-1}$  Mpc.

This requirement reduces the number of available observers in the simulation to 200, observers which we will hereafter call LG-like observers.

### 3.5 Weighting Schemes

We finish this section by discussing the appropriate weighting schemes, to be used in equations (4) and (5), for the various samples. The C sample, being the “parent” population, is volume limited and thus does not suffer from selection effects, so we adopt the direct weight:  $w_i = r_i^{-2}$ . For the R,T-samples, which are flux-limited, we use  $w_i \approx \phi^{-1}(r_i) r_i^{-2}$  to correct for the missing objects. Note that this weighting scheme assumes that the unseen objects follow the same luminosity function and that they are spatially, strongly correlated with the observed objects. Note that for the T-sample we use  $\phi(r) = 1$  for distances between  $7.5h^{-1}$  Mpc and  $45h^{-1}$  Mpc.

## 4 ANALYSIS AND RESULTS

We compute the moments of the cluster distribution for all 3 samples (C, R, T), in bins of  $20h^{-1}$  Mpc width. We sum the contributions from all objects up to  $R_{\max} = 480h^{-1}$  Mpc using periodic boundary conditions.

### 4.1 Monopoles

We plot in fig. 2 the average random observer monopoles, for all three sets of clusters calculated according to equation (4), which as expected increase linearly with  $r$ . For the flux-limited (R and T) samples, however, we observe a systematic early flattening at  $\sim 100h^{-1}$  Mpc, which induces an overall underestimation of the “parent” population (C) monopole, although they are boosted up by using the appropriate correction factor  $\phi^{-1}(r_i)$ . Their relative underestimation of the “parent”-population monopole, measured at depths  $R \geq R_{\text{conv}}$ , is  $\delta M \approx 10$  and 20 per cent respectively for the T and R samples. This implies that the mean density of X-ray clusters, calculated using the flux-limited sample monopole (via  $\bar{n} = M/4\pi R$ ), would be an underestimate of their true underlying mean density, which would then provide an artificially lower estimate of  $\beta$  in equation (7). We note that, up to  $100h^{-1}$  Mpc, we expect on average  $\approx 50 - 60$  clusters.

### 4.2 Dipole as a function of distance

To study the similarities of the different sample dipoles shape we use the usual correlation coefficient analysis (see equation 17 of K96). Furthermore to examine the accuracy with which the “parent” cluster distribution is traced by the flux-limited R and T samples, we measure their corresponding velocity (dipole) fluctuations as follows.

$$\Delta V_{i,C}(R) = \frac{V_i(R) - V_C(R)}{V_C(R)} \quad (12)$$

The subscript i corresponds to either R or T-samples and the subscript C corresponds always to our “parent” cluster sample (see also equation 18 of K96). Evidently, if the “parent” cluster population is adequately traced by flux-limited samples, we would expect to find

$\Delta V_{i,C}(R) \approx 0 \forall R$ , while in the case of missing contributions we would obtain  $\Delta V_{i,C}(R) < 0$ .

As we anticipated for the case of flux limited samples (section 2.3), we have found that in many cases the raw dipoles (before correcting for the shot-noise effects) diverge as a function of depth beyond the depths were their parent 3D cluster dipole has already converged. Therefore, we will present results based on both shot-noise correcting techniques discussed in section 2.3, although we expect that for some observers such a correction will underestimate their true dipole amplitude.

#### 4.2.1 Random observers

In most of the cases the ‘‘parent’’ sample (C) dipole amplitude is constantly higher than that of the T-sample. Note that, in both these cluster sets, the ‘local region’ up to  $45h^{-1}$  Mpc is included. The dipole shapes are quite similar up to  $R_{\max}$ , which is evident from their relative shape correlation coefficient being  $\approx 0.84 \pm 0.13$ . However, the dipole amplitude of the C sample is underestimated by the flux-limited sample, i.e.  $\Delta V_{T,C}(R) \approx -0.18$  and  $-0.1$  for the shot-noise corrected and uncorrected case respectively.

Comparing the C and R dipoles we find  $\Delta V_{R,C}(R) \lesssim -0.3$  and  $-0.2$  for the shot-noise corrected and uncorrected case respectively, while their relative dipole-shape correlation coefficient is  $0.81 \pm 0.12$ . This implies that in many occasions the C dipole is dominated by substantial ‘local’ contributions, within  $(50 - 60)h^{-1}$  Mpc which the R dipole inevitably miss by construction and thus underestimates even further the ‘parent’ population dipole.

Examining the dipole amplitudes of the three cluster samples, we identify the following categories in decreasing order of frequency.

- (i)  $V_C \gg V_T \geq V_R$  in 60 per cent of the observers.
- (ii)  $V_C \approx V_T \approx V_R$  (within 10 per cent) in 30 per cent of the observers and
- (iii)  $V_R > V_C$  in 10 per cent of the cases.

In fig. 3, we plot dipoles for the three samples as a function of radial distance. Panels (a) and (b) are representative of the first category, panel (d) of the second category and panel (c) is of the third case. Most of the R-dipoles underestimates the ‘parent’ population dipole up to a distance of  $\approx 100h^{-1}$  Mpc, where they actually start gaining amplitude. The final convergence comes at  $R_{\text{conv}} \approx 200h^{-1}$  Mpc.

We also plot in fig. 4, the relative velocity fluctuations ( $\Delta V$ ). Note that, in the C versus T case the velocity fluctuation,  $\Delta V_{C,T}(R)$ , convergence to its final value at  $\approx 120h^{-1}$  Mpc, whereas the situation is entirely different for  $\Delta V_{C,R}(R)$ , as expected from the fact that the local region ( $< 45h^{-1}$  Mpc) has been excluded in the R sample. Here at depths below  $100h^{-1}$  Mpc, we observe a very low value  $\Delta V_{C,R}(R) \approx -0.6$ , which reaches its final value ( $\approx -0.3$ ) at  $R \approx 180h^{-1}$  Mpc.

It is important to note that, had we not corrected at all for the shot-noise effects (section 2.3) we would have found lower underestimates of the parent cluster

dipole amplitude (i.e.  $\Delta V(R) \approx -0.1 \sim -0.2$ ) as expected from the fact that our shot-noise correction is maximal (see discussion in section 2.3). In general, this indicates that the underestimation of the true underlying cluster dipole amplitude by the flux-limited samples is counteracted at some level by the artificial dipole amplitude enhancement due to the shot-noise effects. The shot-noise correction is however very important in order to identify the true dipole convergence depth.

#### 4.2.2 LG-like observers

Using equation (12) we find similar  $\Delta V$  values as in the random observer case (i.e.  $\Delta V_{T,C}(R_{\text{conv}}) \approx -0.16$  and  $\Delta V_{R,C}(R_{\text{conv}}) \approx -0.3$ ), which again represent an underestimate of the C-dipole. However, the correlation coefficients of the dipole shapes are systematically larger in this case than for the random observers. We find  $0.9 \pm 0.1$  for the C versus T samples and  $0.87 \pm 0.09$  for the C versus R ones. It is clear that, the three dipoles are in good agreement, as far as their shapes are concerned.

We can break down the behavior of the dipole amplitude for the LG-like observers into the same categories as for the random observers case. Only slight changes occur in the relative frequencies with most notable the slight increase of the observers for which their flux-limited samples provide good estimates of the ‘parent’-population cluster dipole (C) ( $\sim 40$  per cent of total). We do not present plots for the LG-like observers due to their qualitative similarity with those of the random observers (figs 3 and 4).

Finally, we report that for both sets of observers we have also applied the classical shot-noise correction of section 2.3. Although we do not show any plots for reasons of brevity, results clearly suggest that whatever the adopted method for such corrections, both flux-limited cluster samples (R, T) underestimate the ‘parent’ (3D) dipole by at least 10 per cent independently of the observer.

### 4.3 Dipole alignment

In fig. 5 we present the relative dipole misalignment angles,  $\Delta\theta$ , between the three sample dipoles, averaged over the ensemble of all observers. We define  $\Delta\theta_{C,T}$  to be the misalignment angle between the dipole vectors of the C and T samples, and  $\Delta\theta_{C,R}$  between C and R. Panel (a) shows the  $\Delta\theta$  as a function of distance for the random observers while panel (b) for the LG-like observers.

For the random observers, we obtain mean values of  $\Delta\theta_{C,T} \sim 18^\circ \pm 15^\circ$  and  $\Delta\theta_{C,R} \sim 47^\circ \pm 30^\circ$ . The above numbers have been measured at  $R_{\text{conv}}$ . The big difference of  $\approx 30^\circ$  in the mean misalignment angles between  $\Delta\theta_{C,T}$  and  $\Delta\theta_{C,R}$  can be attributed to the fact that the R dipole ignores (by construction) the local region ( $< 45h^{-1}$  Mpc). This again shows how important the ‘local region’ actually is in determining the cluster dipole. From panel (a) of fig. 5, it is clear that the misalignment angle between the C and T sample dipoles converge to its final value at  $\sim 100h^{-1}$  Mpc while between the C

and R-dipoles this scale is  $\sim 200h^{-1}$  Mpc. For distances well below this limit, we get  $\Delta\theta \sim (60^\circ - 70^\circ)$ .

As seen from panel (b), the situation is greatly improved, when we use the LG-like observers, since by construction their dipole properties are not dominated only by the ‘local region’. The large misalignment angles are reduced rapidly and converge to a significantly lower value at  $\sim 150h^{-1}$  Mpc. We obtain  $\Delta\theta_{C,T} \approx 17^\circ \pm 11^\circ$  with a median of  $18^\circ$  and  $\Delta\theta_{C,R} \approx 30^\circ \pm 20^\circ$  with a corresponding median of  $31^\circ$ .

Note, finally, that we did not apply any correction for shot-noise effects in the dipole direction analysis. A shot-noise correction is expected to reduce the dipole misalignment angle by at least  $10^\circ$ .

#### 4.4 A Cluster Bias Estimate

Using equation (7) and the input value of  $\Omega_o (= 1)$ , given by the model we simulate, we can estimate the cluster bias parameter, via:

$$b_c = \frac{1}{N} \sum_{i=1}^N \frac{|V|_{c,i}(R)}{|u|_i(R)}, \quad (13)$$

where  $N$  is the total number of observers used and  $R \geq R_{\text{conv}}$ . The small subscript  $c$  indicates cluster velocity for the three samples (see section 3.3 and equation 7), whereas  $i$  shows the specific observer used in the summation. A more elaborate version of this procedure was tested and found to provide a reliable estimate of  $b_c$  in K96. Using equation (13) and those LG-observers for which their peculiar velocity vector lie within  $\sim 25^\circ$  of their measured cluster dipole we obtain for the ‘‘parent’’ sample:

$$b_c = 4.8 \pm 1.5, \quad (14)$$

a value which is very similar to that derived by the ratio of the cluster to dark-matter variances (measured on scales  $> 50h^{-1}$  Mpc). However the method of equation (13) produces a large observer-to-observer scatter (6 to 8 times larger than in variance method) which is the outcome of the fact that the very local contributions to the dynamics of some observers may not be represented in the cluster distribution, since these can be due to the very local inhomogeneities in the matter distribution.

The underestimation of the ‘‘parent’’-population dipole amplitude by the flux-limited samples will inevitably reflect itself on an artificially lower bias parameter, given by equation (13). In fact we obtain  $b_c \approx 3.95 \pm 1.6$  and  $3.45 \pm 1.4$  for the T and R samples respectively.

#### 4.5 Summary of Moment Analysis

The flux-limited cluster samples underestimate the X-ray ‘‘parent’’ population dipole. All dipoles are in good agreement (within 10 per cent), in about only one in three cases. The main effect of imposing a flux-limit is a general loss of dipole amplitude, which amounts to 10/20 per cent for the T sample and up to 20/30 per cent for the R sample (depending on whether one corrects or not for shot-noise effects). Note that the above results

are independent of the two methods used (discussed in section 2.3) to correct for the shot-noise effects. The relative difference between the two flux-limited samples (which can reach a maximum amplitude of  $\sim 15$  per cent) is due to the exclusion of the ‘local region’ from the R sample, which corresponds to the inability of the RASS to sample the local extended X-ray cluster sources. The misalignments between the flux-limited sample dipoles and that of the ‘‘parent’’-population are quite large, ranging from  $20^\circ$  to  $47^\circ$  on average (for the T and R samples respectively).

If we restrict our analysis to those observers that have a ‘‘parent’’ cluster population that exhibits a similar dipole to the observed Abell/ACO cluster case (i.e. having significant contribution from large scales; cf. Branchini & Plionis 1996), the two flux-limited samples have dipole directions in much better agreement with that of the ‘‘parent’’ cluster dipole ( $\Delta\theta \sim 17^\circ$  and  $30^\circ$  respectively for the T and R samples). The dipole amplitude underestimation by the flux-limited samples is however of a similar amplitude as in the random observers case.

Note, importantly, that the underestimation of the ‘‘parent’’ cluster dipole amplitude by these flux-limited samples compared would lead, using equation (7), to an incorrectly higher estimate of the  $\beta_c$  parameter and thus to either an artificially higher value of  $\Omega_o$  for a specific value of  $b_c$  or to an artificially lower value of  $b_c$  for a specific value of  $\Omega_o$ .

## 5 X-RAY CLUSTER CONTRIBUTION TO XRB

### 5.1 A brief overview

Since it was brought forward by Giacconi et al. (1962), the XRB has been something of an enigma for theoretical cosmology. Its origin and its major constituents are still debatable nowadays, and it is still unclear how much of it is contributed by resolved sources and how much by a discrete component (see review by Zamorani 1993 as well as Hasinger et al. 1993; Hasinger 1992; Hasinger 1995). The diffuse hypothesis (thermal breemstrahlung hot plasma with  $T \approx 40$  keV) has largely been abandoned, because such a hot component would generate severe distortion on the CMB spectrum, which is not detected by COBE. The alternative solution of assuming that the XRB is made up of the integrated X-ray flux from discrete objects is more attractive, but as yet no specific class of sources has been found with a spectrum identical to that of the XRB.

Setting the spectral difficulties to one side, we shall attempt to quantify the contribution to the XRB from clusters of galaxies. Many similar attempts have been made for various other sources (active galaxies, QSOs) as well as clusters, in both soft ( $E \leq 2$  keV) and hard ( $E > 2$  keV) energy bands; see Shanks et al. (1991) (and references therein), Blanchard et al. (1992), Georgantopoulos et al. (1993), Boyle et al. (1994), Roche et al. (1995) (and references therein) for the QSO contribution to the soft XRB, Lahav et al. (1993) (and references therein) discuss the contribution from galaxies,



Anvi (1978) and Maccacaro et al. (1984) have discussed the case for AGN and Piccinotti et al. (1982), Gioia et al. (1990), McKee et al. (1980), Schwartz (1978), Henry et al. (1992), Soltan et al. (1995), Kitayama & Suto (1996), Kitayama, Sasaki & Suto (1997) and Oukbir, Bartlett & Blanchard (1997) are mostly concerned about X-ray clusters.

We will attempt to estimate the contribution of X-ray clusters, having a X-ray luminosity function given by equation (9) to the soft XRB using two simple methods (see Maccacaro et al. 1984, their section 4), not worrying for the different cosmological backgrounds that could affect the detailed modelling of such contribution (cf. Kitayama & Suto 1996; Kitayama et al. 1997). Note that the present application holds only for a flat model with vanishing  $\Lambda$  term, since this is the background that de Grandi (1996) has assumed in deriving the relative parameters of the ESO-KP X-ray luminosity function.

## 5.2 Luminosity Function Method

First we compute the contribution of X-ray clusters either in terms of flux per steradian or in terms of luminosity density ( $\text{erg s}^{-1} h \text{Mpc}^{-3}$ ). In other words, we compare either intensities of clusters and XRB, or volume emissivities at a given energy band. The contribution of clusters is estimated integrating the product  $L \Phi(L)$ :

$$J_c = \int_{L_{\min}}^{L_{\max}} L \Phi(L) dL, \quad (15)$$

where  $L_{\min} \approx 4 \times 10^{41} h^{-2} \text{erg s}^{-1}$  and  $L_{\max} \approx 10^{45} h^{-2} \text{erg s}^{-1}$  (see section 2.2). The quantity  $J_c$  expresses the integrated cluster volume emissivity. Since there is no clear picture which describes the corresponding volume emissivity of the XRB in such a soft band, we will simply be using the well-defined intensity of the XRB in the 1-2 keV band, namely  $I_X \approx 1.25 \times 10^{-8} \text{erg s}^{-1} \text{cm}^{-2} \text{sr}^{-1}$  of Hasinger et al. (1993), as the basis of our estimate. Assuming values for the spectral index of the soft XRB in the usual range of 1-1.2, we first convert the latter value in the monochromatic band (at 1.5 keV) and then we use a conversion factor to transform it to the 0.1-2.4 keV one. Such a calculation yields  $I_X \approx 4 \pm 0.2 \times 10^{-8} \text{erg s}^{-1} \text{cm}^{-2} \text{sr}^{-1}$  (0.1-2.4 keV), for the XRB intensity in the usual ROSAT band. Evidently, we should compare intensities with luminosities in identical bands and for this purpose we either convert the cluster volume emissivity in flux, or the intensity of the XRB in light density units. The former requires an accurate knowledge of the spectral index of X-ray clusters, for the conversion to be valid. We will assume a typical value for the spectral index of X-ray clusters in the soft band of the order of 0.4 (photon index 1.4). The relation between volume emissivities and intensities (Schwartz & Gorsky 1974; Anvi 1978; Soltan et al. 1995) is given by

$$I_i = \frac{c J_i}{4 \pi H_o} \int_0^{z_{\max}} \frac{(1+z)^{1-\alpha_i}}{(1+z)^3 \sqrt{1+2q_o z}} dz. \quad (16)$$

The subscript  $i$  corresponds to the objects under study; one can use equation (16) interchangeably for  $I_i$  or  $J_i$ . The look-back integral depends on parameters such as  $H_o, q_o$  and  $\alpha_i$  (a zero cosmological constant is assumed). Varying  $q_o$  in the range between 0.1 and 0.5 does not affect the the look-back time integral by more than 10 per cent. The cluster contribution to the soft XRB, if  $q_o$  is in the above range, is therefore well within the uncertainties quoted throughout this section. Furthermore the dependence on  $H_o$  drops out from the final result. Using the spectral index of the XRB given above, we can solve for  $J_X$ . The upper limit of the integral presents the maximum distance up to which, sources generate the XRB. Values between 3, 4 and  $\infty$  do not influence the final results by more than 3 per cent. In what follows we will be using  $z_{\max} = 4$  and  $q_o = 0.5$ . We then obtain from equation (16) that  $J_X \approx 4.1 \pm 0.1 \times 10^{39} \text{erg s}^{-1} h \text{Mpc}^{-3}$  (0.1-2.4 keV). Adopting the corresponding value for the clusters (equation 15), we can express the fractional contribution of X-ray clusters to the total of the soft XRB as

$$\mathcal{C}_{0.1-2.4 \text{ keV}} = \frac{J_c}{J_X} \approx (9 \pm 1) \%, \quad (17)$$

which is independent of the value of  $H_o$ .

We can obtain another estimate of  $\mathcal{C}_{0.1-2.4 \text{ keV}}$ , starting with the formalism of Schwartz & Gorsky (1974), using equation (16) and the spectral intensity of the XRB for energies between 1 keV and 21 keV and then solving for  $J_X$ . The spectral intensity is expressed as:

$$I(E) \approx 8.5 E^{-0.4} \frac{\text{keV}}{\text{keV cm}^2 \text{s sr}}, \quad (18)$$

for  $1 \leq E \leq 21$  in keV's. It is apparent though, that such a scheme does not cover the lower limit of our soft band (at 0.1 keV). We can circumvent, however, this difficulty by using the following alternatives. The first is to extrapolate the shape of the spectrum at low energies, so as to match our lower bound, and the second is to perform calculations in the perfectly allowed (1-2 keV) band, which we later convert in the soft ROSAT one as before. We choose the second method, since it does not violate the energy range and it appears to be more realistic. However, the former method produces figures always within  $\pm 1\sigma$  of the latter. We caution the reader that there is no well-known  $I(E)$  for the band we are interested in and this energy range is mostly unexplored in terms of spectrum. Taking again the same set of parameters as before ( $H_o, q_o, \alpha_X, I_X$ ), we obtain  $J_X \approx 3.95 \pm 0.1 \times 10^{39} \text{erg s}^{-1} h \text{Mpc}^{-3}$  (0.1-2.4 keV), which is in good agreement with the value previously computed and which gives  $\mathcal{C}_{0.1-2.4 \text{ keV}} \approx (10 \pm 1) \%$ . Note that the errors of both estimates reflect the uncertainty of the choice of the spectral index of the soft XRB, being used in equation (16) (cf. Soltan et al. 1995).

A further estimate of  $\mathcal{C}_{0.1-2.4 \text{ keV}}$  is obtained using an estimate of the spectral index of clusters of the order of  $\alpha_c = (0.4 - 0.5)$ , as in Maccacaro et al. (1988), and using the value of  $J_c$  from equation (15) in the 0.1-2.4 keV band, we can then solve equation (16), this time for the total intensity for X-ray

clusters,  $I_c$ , in the same energy range. We find that  $I_c \approx 4.5 \pm 0.1 \times 10^{-9} \text{ erg s}^{-1} \text{ cm}^{-2} \text{ sr}^{-1}$  (0.1-2.4 keV). By comparing this with the previous estimate of  $I_X$  (0.1-2.4 keV), we find

$$\mathcal{C}_{0.1-2.4 \text{ keV}} = \frac{I_c}{I_X} \approx (11 \pm 1) \% \quad (19)$$

consistent with the previous estimates. For all the above estimates, we have assumed that the spectral indices of both clusters and XRB are not subject to any change when passing from one energy band to another and although a few such assumptions have been used, this framework does yield consistent results.

### 5.3 Number-Flux Distribution Method

A different approach is used here, which is independent of the value of  $q_0$ , that enters in the evaluation of the look-back integral. We assign a random luminosity to each simulated cluster using the X-ray luminosity function of equation (9), which we then convert to a flux using its distance. For this, we use the constant multiplier of de Grandi (1996) to transform 0.5-2 keV fluxes (or luminosities) to the broad 0.1-2.4 keV band (as discussed in section 2.2). Note that the particular CHDM simulation we use is irrelevant to this analysis; we could have even used a Monte-Carlo cluster distribution provided that the  $N(r)$  distribution, predicted by the X-ray cluster selection function, would be preserved. We plot in fig. 6 the distribution of X-ray luminosities as a function of distance. The solid line corresponds to the imposed flux limit of  $1.5 \times 10^{-12} \text{ erg s}^{-1} \text{ cm}^{-2}$ , for any given distance. The plot shows results for a single observer; we have verified that this behavior of the distribution is entirely independent of the observer position.

Having obtained the fluxes of the  $\sim 1300$  X-ray-like clusters, we simply add their individual contributions towards the total cluster X-ray emission in the corrected soft band. To estimate the scatter due to sampling effects we use 500 random observers from the initial ensemble and we repeat the procedure for each number-flux relation. We report results, as usual, as the mean and the  $\pm 1\sigma$  errors. We find that,  $I_c \approx 4.25 \pm 0.3 \times 10^{-9} \text{ erg s}^{-1} \text{ cm}^{-2} \text{ sr}^{-1}$  (0.1-2.4 keV). We compare intensities of clusters and XRB as computed in section 5.2. We obtain  $\mathcal{C}_{0.1-2.4 \text{ keV}} \approx 10.5 \pm 1$  per cent for the contribution of the discrete set of these clusters. Alternatively, we can again assume equation (16) and the same spectral index for clusters, in order to convert fluxes per unit area to volume emissivities. This approach yield identical results.

However, since we have used our simulated catalogue which is limited to a radius of  $480h^{-1} \text{ Mpc}$ , we need to take into account the contribution of the extra  $\sim 300$ -400 clusters predicted by the X-ray cluster selection function to lie  $z \gtrsim 0.16$ , which we estimate to be no more than 1.5 per cent of the previously quoted value. Therefore this estimate is in very good agreement with our previous findings (see equations 17 and 19).

We, therefore, quote the contribution of clusters to the soft XRB, as an average of the two methods used above. This yields

$$\mathcal{C}_{0.1-2.4 \text{ keV}} \approx (10 \pm 2) \% \quad (20)$$

with quoted uncertainty covering the  $1\sigma$  deviations of all previously computed averages. A similar value was obtained recently by Oukbir et al. (1997).

## 6 CONCLUSIONS

We have used numerical simulations of the cluster distribution and the de Grandi (1996) X-ray cluster luminosity function, to create samples of X-ray type clusters. We investigate their relative dipole properties, by paying particular attention to what extent the underlying ‘‘parent’’ population cluster dipole can be recovered by the flux-limited subsamples.

We analysed the results based on 2 different sets of observers; random observers and those that have a cluster dipole structure in reasonable agreement with that of the Abell/ACO clusters (LG-like observers). We found that on average the ‘‘parent’’ cluster dipole is underestimated by  $\sim 20/30$  per cent in the former type of observers and slightly less,  $\sim 10/20$  per cent, in the latter type (for the raw and shot-noise corrected cases respectively). However, the profile of the ‘‘parent’’ dipole amplitude as well as the dipole direction is much better recovered in the LG-like observer case ( $\Delta\theta \sim 30^\circ$  and  $47^\circ$  respectively for the LG-like and random observers). We also found that the exclusion from the flux-limited X-ray cluster samples of the local region ( $\lesssim 45h^{-1} \text{ Mpc}$ ), as is the case with RASS, will result into larger underestimates of the ‘‘parent’’ dipole amplitude and larger misalignments of the dipole directions.

The generic loss of dipole amplitude will be important in interpreting cosmological information coming from samples of X-ray selected clusters, such as their relative bias factor and the inferred values of  $\Omega_0$ .

Finally, we attempted to estimate the contribution of these X-ray clusters to the soft (0.1-2.4 keV) XRB for the particular case of a flat universe with  $\Omega_\Lambda = 0$ . We use the standard method for deriving the cluster volume emissivity, as well as that using the cluster number-flux relation. The fractional contribution of clusters to the soft ROSAT energy band is estimated to be  $10 \pm 2$  per cent, using both techniques.

**Note added in Manuscript:** When this project was in its final stages, two new X-ray flux-limited cluster samples appeared in the literature, namely the X-ray Brightest Abell-type Cluster sample (XBACs; Ebeling et al. 1996b) and Brightest Cluster Sample (BCS; Ebeling et al. 1997a and Ebeling et al. 1997b). The XBACs sample consist of 242 Abell/ACO X-ray clusters above the limiting flux of  $5 \times 10^{-12} \text{ erg s}^{-1} \text{ cm}^{-2}$  and it is the biggest all-sky X-ray cluster list, up till now. The BCS (largest in the northern hemisphere) comprises 199 X-ray Abell, Zwicky as well as other purely X-ray selected systems, being flux-limited above  $4.45 \times 10^{-12} \text{ erg s}^{-1} \text{ cm}^{-2}$ . Both samples are selected at high galactic latitudes ( $|b| \gtrsim 20^\circ$ ) and in the same soft energy band (0.1-2.4 keV). In both samples the cluster

identification procedure is mostly based on the Voronoi Tessellation Percolation (VTP) algorithm (see also Allen et al. 1992; Ebeling & Wiedenman 1993; Crawford et al. 1995), which not only samples nearby extended X-ray emission much more adequately than the SASS algorithm, but also increases significantly the accuracy with which fluxes are computed. This, together with the fact that their depth coverage is large ( $z \sim 0.2$  and  $0.3$  for XBACs and BCS respectively), renders both samples ideal tools for large scale structure studies. These catalogues together with the forthcoming ESO KP will definitely constitute three of the more significant X-ray databases for future cosmological research. We, therefore, intend to study these samples extensively along the lines set in this work.

### ACKNOWLEDGMENTS

VK receives a PPARC research studentship. PC is a PPARC Advanced Research Fellow. We benefited greatly from endless discussions with Luigi Guzzo regarding some crucial observational features of the ESO KP and from his productive criticism on a late draft of this work. We also thank Enzo Branchini for various useful suggestions and Dimitra Rigopoulou and Sabrina de Grandi for invaluable information on some parts of this work. VK also acknowledges fruitful discussions with Jacob Sharpe and Ioannis Georgantopoulos. Special thanks to Harald Ebeling for the long and instructive comments about several aspects of the ROSAT surveys and cluster identification procedures and for reading carefully an early version of the present paper. This work has been partially supported by funds originating from the EC Human Capital and Mobility Network (Contract Number CHRX-CT93-0129).

### REFERENCES

- Allen S.W. et al. 1992, MNRAS, 259, 67  
 Anvi Y., 1978, A&A, 63, L13  
 Blanchard A., Wachter K., Evrard A.E., Silk J., 1992, ApJ, 391, 1  
 Borgani S., Coles P., Moscardini L., 1994, MNRAS, 271, 223  
 Borgani S., Plionis M., Coles P., Moscardini L., 1995, MNRAS, 277, 1191  
 Borgani S. et al., 1997, NewA, 1, 321  
 Boyle B.J., Griffiths R.E., Shanks T., Stewart G.C., Georgantopoulos I., MNRAS, 1994, 271, 639  
 Branchini E., Plionis M., 1996, ApJ, 460, 569  
 Cen R., 1997, ApJ, in press  
 Coles P., 1993, MNRAS, 262, 1065  
 Collins C.A. et al., 1995, in Maddox S.J., Aragon-Salamanca A., eds, Wide field spectroscopy and the distant universe: The 35th Herstmonceux Conference. World Scientific (Singapore), p. 213  
 Collins C.A., Burke D.J., Romer A.K., Sharples R.M., Nichol R.C., 1997, ApJ, in press  
 Crawford C.S., Edge A.C., Fabian A.C., Allen S.W., Böhringer H., Ebeling H., McMahon R.G., Voges W., 1995, MNRAS, 274, 75  
 Davis M., Huchra J.P., 1982, ApJ, 254, 437  
 de Grandi S., 1996, in Zimmermann H.U., Trümper J., eds, Röntgerstrahlung from the universe: International conference on X-ray Astronomy and Astrophysics. Würzburg, Germany, p. 577  
 de Grandi S., Molendi S., Böhringer H., Chincarini G., Voges W., 1997, ApJ, in press  
 Dalton G.B., Croft R.A.C., Efstathiou G., Sutherland W.J., Maddox S.J., Davis M., 1994, MNRAS, 271, L47  
 Ebeling H., Wiedenmann G., 1993, Physical Review E, 47, 704  
 Ebeling H. et al., 1995, in Maddox S.J., Aragon-Salamanca A., eds, Wide field spectroscopy and the distant universe: The 35th Herstmonceux Conference. World Scientific (Singapore), p. 221  
 Ebeling H., Allen S.W., Crawford C.S., Edge A.C., Fabian A.C., Böhringer H., Voges W., Huchra J.P., 1996a, in Zimmermann H.U., Trümper J., eds, Röntgerstrahlung from the universe: International conference on X-ray Astronomy and Astrophysics. Würzburg, Germany, p. 579  
 Ebeling H., Voges W., Böhringer H., Edge A.C., Huchra J.P., Briel U.G., 1996b, MNRAS, 281, 799  
 Ebeling H., Edge A.C., Fabian A.C., Allen S.W., Crawford C.S., 1997a, ApJ, 479, L101  
 Ebeling H., Edge A.C., Böhringer H., Allen S.W., Crawford C.S., Fabian A.C., Voges W., Huchra J.P., 1997b, MNRAS, submitted  
 Edge A.C., Stewart G.C., Fabian A.C., Arnaud K.A., 1990, MNRAS, 245, 559  
 Edge A.C., Stewart G.C., 1991, MNRAS, 252, 414  
 Georgantopoulos I., Stewart G.C., Shanks T., Boyle B.J., Griffiths R.E., 1993, MNRAS, 262, 619  
 Giacconi R., Gursky G.R., Paolini F.R., Rossi B.B., 1962, Phys. Rev. Letters, 9, 439  
 Gioia I.M., Henry J.P., Maccacaro T., Morris S.L., Stocke J.T., Wolter A., 1990, ApJ, 356, L35  
 Gioia I.M., 1996, in Coles P., Martinez V.J., Pons-Borderia Maria-Jesus., eds, Mapping, measuring and modeling the universe. ASP Conference series, Vol. 94, p. 209  
 Górsky K. et al., 1994, ApJ, 430, L89  
 Guzzo L. et al., 1995, in Maddox S.J., Aragon-Salamanca A., eds, Wide field spectroscopy and the distant universe: The 35th Herstmonceux Conference. World Scientific (Singapore), p. 205  
 Guzzo L., 1996, in Coles P., Martinez V.J., Pons-Borderia Maria-Jesus., eds, Mapping, measuring and modeling the universe. ASP Conference series, Vol. 94, p. 157  
 Hasinger G., 1992, in Barcons X., Fabian A.C., eds, The X-ray background. Cambridge Univ. Press, Cambridge, p. 229  
 Hasinger G., Burg R., Giacconi R., Hartner G., Schmidts M., Trümper J., Zamorani G., 1993, A&A, 275, 1  
 Hasinger G., 1995, in Maddox S.J., Aragon-Salamanca A., eds, Wide field spectroscopy and the distant universe: The 35th Herstmonceux Conference. World Scientific (Singapore), p. 321  
 Henry J.P., Gioia I.M., Maccacaro T., Morris S.L., Stocke J.T., Wolter A., 1992, ApJ, 386, 408  
 Juskiewicz R., Vittorio N., Wyse R.F.G., 1990, ApJ, 349, 408  
 Kaiser N., 1984, ApJ, 284, L9  
 Kitayama T., Suto Y., 1996, MNRAS, 280, 638  
 Kitayama T., Sasaki S., Suto Y., 1997, PASJ, submitted  
 Kolokotronis V., Plionis M., Coles P., Borgani S., Moscardini L., 1996, MNRAS, 280, 186 (K96)  
 Klypin A., Rhee G., 1994, ApJ, 428, 399  
 Lahav O., Edge A.C., Fabian A.C., Putney A., 1989, MNRAS, 238, 881  
 Lahav, O., Kaiser N., Hoffman Y., 1990, ApJ, 352, 448  
 Lahav O. et al., 1993, Nature, 364, 693

- Maccacaro T., Gioia I.M., Stocke J.T., 1984, *ApJ*, 283, 486  
Maccacaro T., Gioia I.M., Wolter A., Zamorani G., Stocke J.T., 1988, *ApJ*, 326, 680  
McKee J., Mushotzky R., Boldt E., Holt S.S., Marshall F.E., Pravdo S., Serlemitsos P.J., 1980, *ApJ*, 242, 843  
Miyaji T., Boldt E., 1990, *ApJ*, 353, L3  
Moscardini L., Branchini E., Tini Brunozzi P., Borgani S., Plionis M., Coles P., 1996, *MNRAS*, 282, 384  
Nichol R.C., Holden B.P., Romer A.K., Ulmer M.P., Burke D.J., Collins C.A., 1997, *ApJ*, in press  
Oukbir J., Bartlett J.G., Blanchard A., 1997, *A&A*, 320, 365  
Peebles P. J. E., 1980. *The Large Scale Structure of the Universe*, Princeton University Press, Princeton New Jersey  
Piccinotti G., Mushotzky R.F., Boldt E.A., Holt S.S., Marshall F.E., Serlemitsos P.J., Shafer R.A., 1982, *ApJ*, 253, 485  
Plionis M., 1995, in Balkowsky C., Maurogordato S., Tao C., Tr n Thanh V n J., eds, *Proc. of the Moriond Astrophysics Meeting on Clustering in the Universe*, in press  
Plionis M., Valdarnini R., 1991, *MNRAS*, 249, 46  
Roche N., Shanks T., Georgantopoulos I., Stewart G.C., Boyle B.J., Griffiths R.E., 1995a, *MNRAS*, 273, L15  
Romer A.K., Collins C.A., B hringer H., Cruddace R.G., Ebeling H., MacGillivray H.T., Voges W., 1994, *Nature*, 372, 75  
Romer A.K., Nichol R.C., Collins C.A., Burke D.J., Holden B.P., Metevier A., Ulmer M.P., Pildis R., 1997, preprint astro-ph/9701233  
Rosati P., Della Ceca R., Burg R., Norman C., Giacconi R., 1995b, *ApJ*, 445, L1  
Scaramella R., Vettolani P., Zamorani G., 1991, *ApJ*, 376, L1  
Schwartz D.A., 1978, *ApJ*, 220, 8  
Schwartz D.A., Gursky H., 1974, in Giacconi R., Gursky H., eds, *X-ray Astronomy*. Dordrecht, Reidel, p. 359  
Schindler S. et al., 1995, *A&A*, 299, L9  
Shandarin S.F., Zel’dovich Ya.B., 1989, *Rev. Mod. Phys*, 61, 185  
Shanks T., Georgantopoulos I., Stewart G.C., Pounds K.A., Boyle B.J., Griffiths R.E., 1991, *Nature*, 353, 315  
Soltan A.M., Hasinger G., Egger R., Snowden S., Tr mper J., 1996, *A&A*, 305, 17  
Strauss M., Yahil A., Davis M., Huchra J.P., Fisher K., 1992 *ApJ*, 397, 395  
Tini Brunozzi P., Borgani S., Plionis M., Moscardini L., Coles P., 1995, *MNRAS*, 277, 1210 (TB95)  
Yahil A., Strauss M., Davis M., Huchra J.P., 1991, *ApJ*, 372, 380  
Zamorani G., 1995, in Calzetti D., Livio M., Madau P., eds, *Proceedings of the meeting on Extragalactic background radiation: A meeting in honour of Riccardo Giacconi*. Cambridge Univ. Press, Space Telescope Science Institute Symposium Series, N. 7, p. 37  
Zel’dovich Ya.B., 1970, *A&A*, 5, 84

**FIGURE CAPTIONS**

**Figure 1.** X-ray selection function for a model ROSAT-like cluster population.

**Figure 2.** The average, over 1500 random observers, monopole as a function of radial distance for the three samples of clusters. Errorbars reflect the observer-to-observer scatter. Filled dots are for “parent” (C) monopoles, open dots are for T monopoles and filled triangles refer to R monopoles.

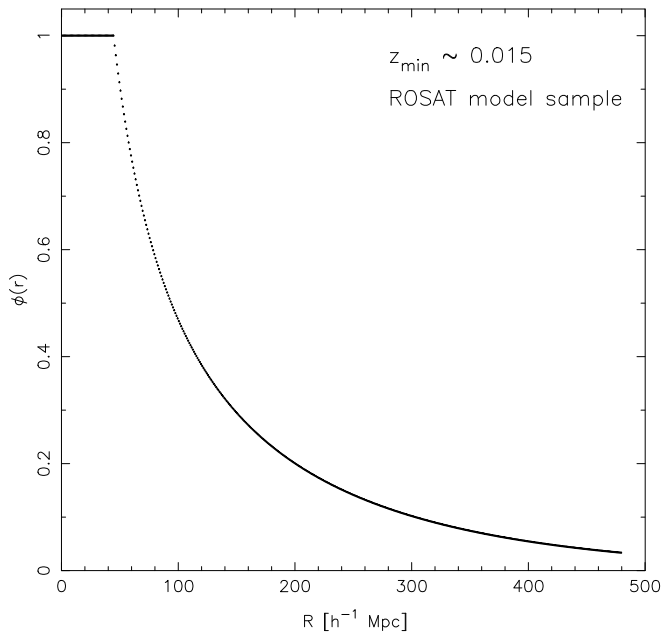
**Figure 3.** Dipole amplitude as a function of radial depth for some characteristic random observers. The solid line corresponds to the R, open circles to the T and filled dots to the “parent” (C) samples. The upper 2 panels represent the most frequent cases, lower right those less frequent and finally the lower left are the rarest of all.

**Figure 4.** Relative velocity fluctuations (equation 14) for the 1500 random observers. Errorbars reflect the observer-to-observer  $1\sigma$  scatter and are shown only for one set of points for clarity. Filled dots correspond to fluctuations between the “parent” and T samples while open dots between the “parent” and R samples.

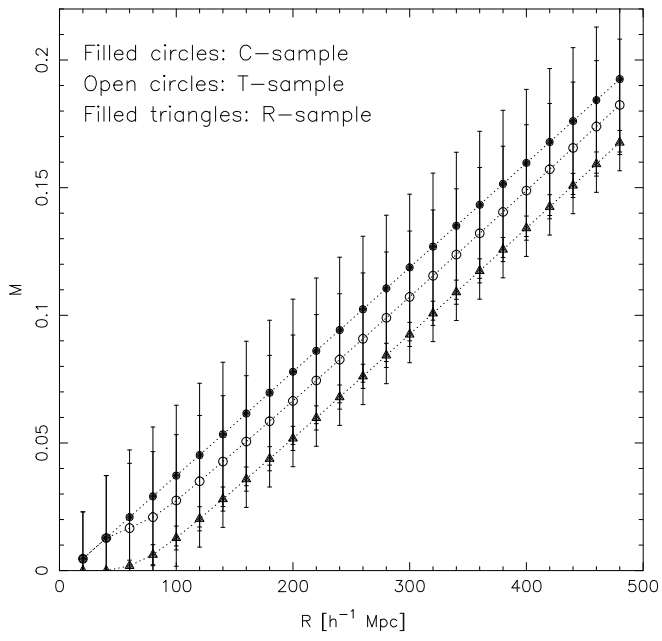
**Figure 5.** Relative misalignment angles,  $\Delta\theta$ . random observer results are shown in panel (a) while those of the LG-like observers are shown in panel (b). Errorbars are only shown for one set of points, in each panel, for clarity. In both panels filled symbols correspond to angular fluctuations between C and R samples, whilst open symbols represent misalignment angles between C and T populations.

**Figure 6.** Luminosity–distance diagram for a model ROSAT-like sample, as viewed by a typical observer. The solid line corresponds to the cut-off introduced due to the flux limit imposed. The plot shows the X-ray cluster distribution of  $\sim 1300$  such objects seen by a specific observer, but the result (shape) is independent of the observer’s choice.

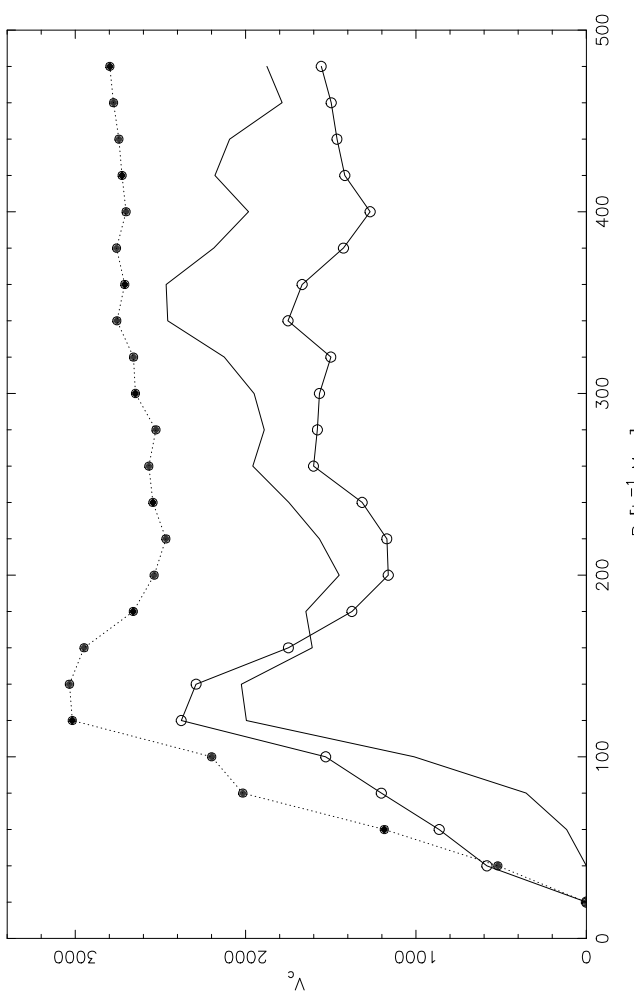
X-ray selection function



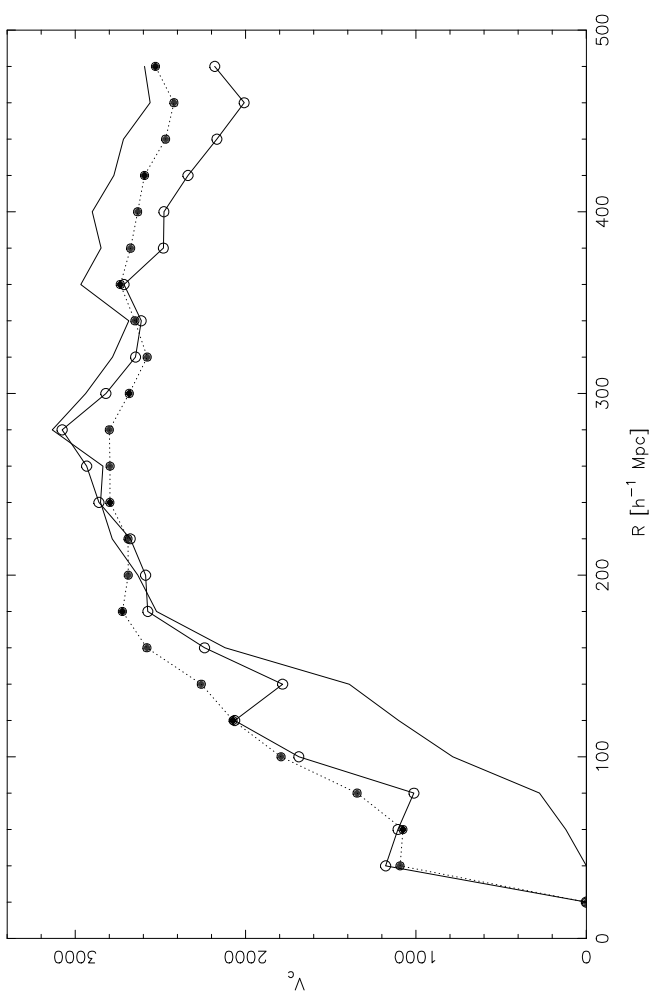
Monopole amplitude



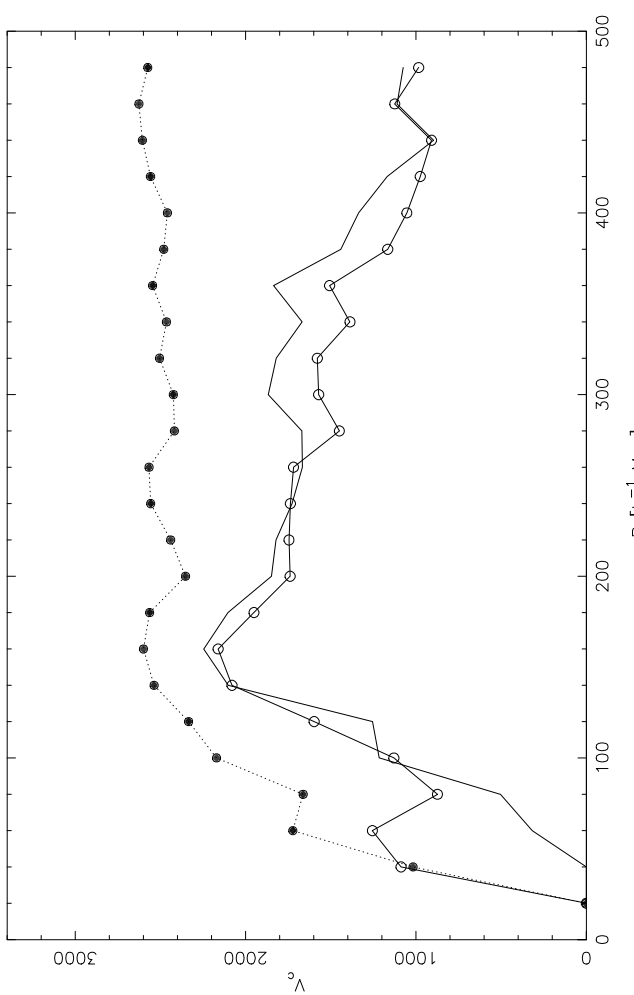
DIPOLE AMPLITUDE



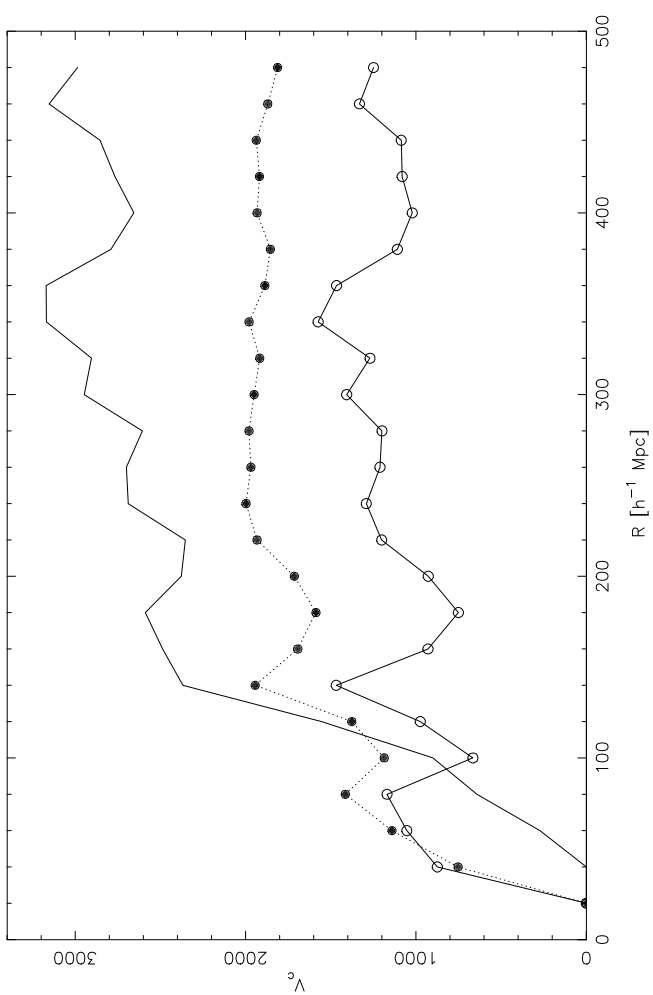
DIPOLE AMPLITUDE

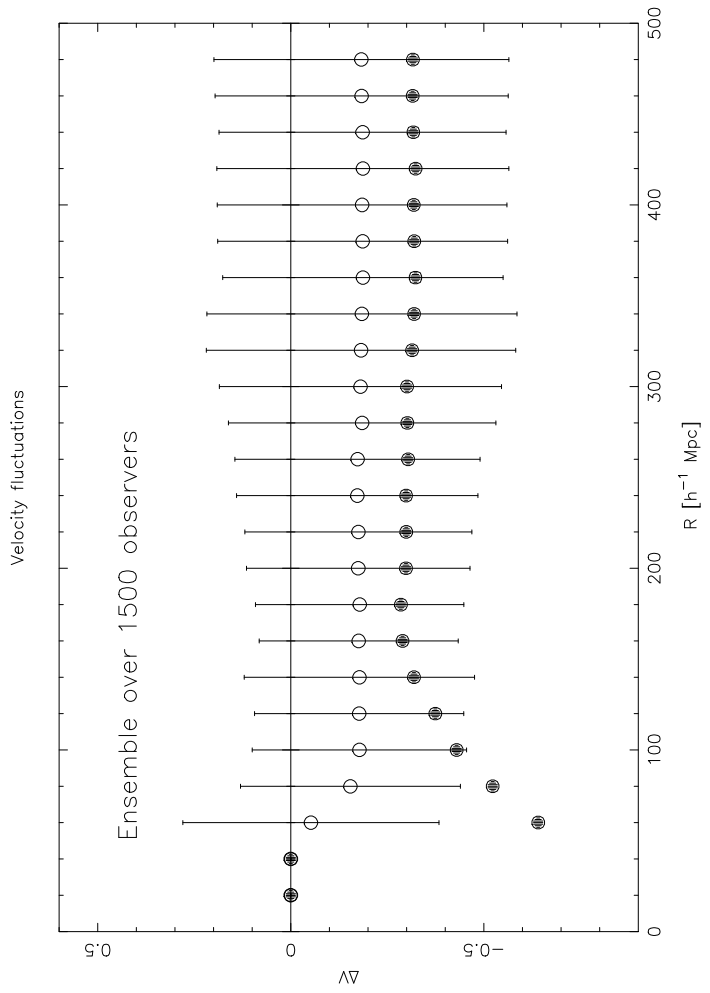


DIPOLE AMPLITUDE



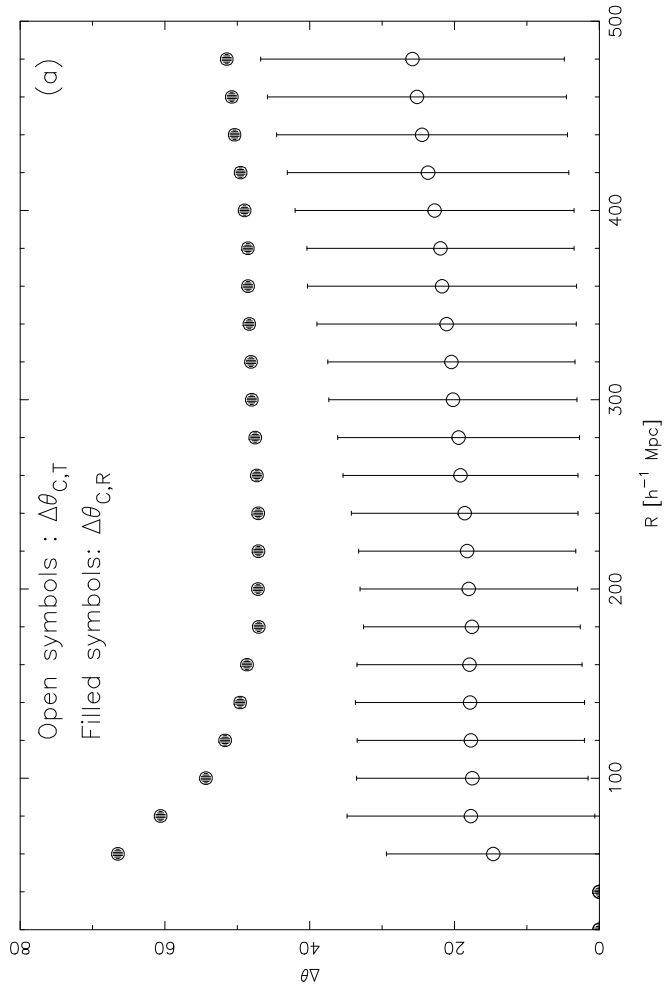
DIPOLE AMPLITUDE







Angular fluctuations



Angular fluctuations

